



Artifact reduction in the CSPAD detectors used for LCLS experiments

Alberto Pietrini^a and Carl Nettelblad^{a,b,*}

^aLaboratory of Molecular Biophysics, Department of Cell and Molecular Biology, Uppsala University, Husargatan 3 (Box 596), Uppsala 751 24, Sweden, and ^bDepartment of Information Technology, Science for Life Laboratory, Uppsala University, Lägerhyddsvägen 2 (Box 337), Uppsala 752 37, Sweden.
*Correspondence e-mail: carl.nettelblad@it.uu.se

Received 31 March 2017

Accepted 18 July 2017

Edited by M. Yabashi, RIKEN SPring-8 Center, Japan

Keywords: CSPAD; detector artifact; LCLS; CXI.

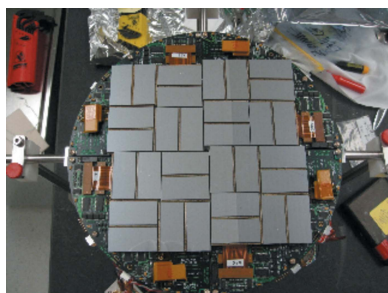
The existence of noise and column-wise artifacts in the CSPAD-140K detector and in a module of the CSPAD-2.3M large camera, respectively, is reported for the L730 and L867 experiments performed at the CXI Instrument at the Linac Coherent Light Source (LCLS), in low-flux and low signal-to-noise ratio regime. Possible remedies are discussed and an additional step in the preprocessing of data is introduced, which consists of performing a median subtraction along the columns of the detector modules. Thus, we reduce the overall variation in the photon count distribution, lowering the mean false-positive photon detection rate by about 4% (from 5.57×10^{-5} to 5.32×10^{-5} photon counts $\text{pixel}^{-1} \text{frame}^{-1}$ in L867, cxi86715) and 7% (from 1.70×10^{-3} to 1.58×10^{-3} photon counts $\text{pixel}^{-1} \text{frame}^{-1}$ in L730, cxi73013), and the standard deviation in false-positive photon count per shot by 15% and 35%, while not making our average photon detection threshold more stringent. Such improvements in detector noise reduction and artifact removal constitute a step forward in the development of flash X-ray imaging techniques for high-resolution, low-signal and in serial nano-crystallography experiments at X-ray free-electron laser facilities.

1. Introduction

Flash X-ray imaging is a novel imaging technique which, when fully developed, will allow diffraction-based imaging experiments on single molecules/particles at X-ray free-electron lasers (XFELs) (Neutze *et al.*, 2000). These light sources have the unique characteristics to support it: highly brilliant (10^9 times greater than any synchrotron) and flat, coherent wavefront pulses (Emma *et al.*, 2010; Jamison, 2010). Proof-of-concept experiments have been conducted at the FLASH facility at DESY (Chapman *et al.*, 2006, 2009; Barlag *et al.*, 2016), at the Linac Coherent Light Source (LCLS) at the SLAC National Accelerator Laboratory (Seibert *et al.*, 2011; Hantke *et al.*, 2014; van der Schot *et al.*, 2015) and at the SACLA facility at SPring-8 (Kimura *et al.*, 2014; Gallagher-Jones & Songa, 2014; Robinson *et al.*, 2015).

In these experiments, biological particles (*e.g.* viruses, bacteria, organelles and cells) suspended in aerosol droplets are injected into a vacuum chamber. The droplets evaporate completely before they reach the interaction point, where they may be hit by a beam pulse, thus causing photon diffraction of an isolated sample in vacuum on a two-dimensional pixelated detector. Signals from individual frames registered by the detector are processed to obtain diffraction patterns, which can then be analyzed to recover the three-dimensional electron density of the particle under study.

The present work reports the presence of a spatially non-uniform artifact in the CSPAD (Cornell-SLAC hybrid Pixel



Array Detector) at the CXI (Coherent X-ray Imaging) beamline at the LCLS. A systematic shift in detector readout along a fixed direction is found and corrected for, resulting in improved photon detection statistics.

1.1. The CXI end-station and the CSPAD and CSPAD 2×2 detectors

A sketch of the CXI end-station is reported in Fig. 1. The experiment chamber used in the data considered in this communication was the 0.1 μm chamber, allowing the study of samples in an interaction region with a nominal 0.1 μm FWHM focal spot (Liang *et al.*, 2015). Inside this chamber there are usually two distinct CSPAD configurations. Each detector is composed of multiple units of the same fundamental component: a CSPAD 2×1 module (388×185 pixels), in which each pixel (size $110 \mu\text{m} \times 110 \mu\text{m}$) reads out a voltage that is proportional to the number of photons scattered on the pixel. The so-called *large camera*, which consists of 64 ASICs (an ASIC being half of a CSPAD 2×1 module), is closest to the interaction point (Fig. 2). This detector provides high-resolution (wide-angle scattering) information. The second detector is located further downstream, typically of the order of 2 m from the interaction point, and is called the *back detector*. It is a CSPAD 2×2 (also called CSPAD-140K) and consists of just four ASICs. It provides low-resolution (small-angle scattering) features.

1.2. Data

The back detector (the cxi73015 experiment, or L730 for short) and a central CSPAD 2×1 module in the large camera [the cxi86715 experiment, or L867 for short, as described by Munke *et al.* (2016)] are the objects of our study. We investigated their performance by analyzing dark and sample runs from these two experiments to detect artifacts. Moreover, we believe our analysis has a general validity for all CSPAD detectors, as they share the same fundamental unit. Even though the two experiments considered were performed two years apart, both used the same CSPAD ASIC revision, 1.6 (Herrmann *et al.*, 2014).

1.3. Identifying per-pixel gain and pedestal values

For low-flux experiments, it is crucial to estimate the exact number of photons hitting each pixel, in order to obtain a reasonable signal-to-noise ratio for further analysis.

Each pixel in a CSPAD detector contains an analog memory cell, a counting register and a comparator. The readout is based on the number of counted ticks before a distributed reference voltage matches the level within the cell (Herrmann *et al.*, 2012). The raw readout of the number of ticks is in arbitrary digital units (ADUs). Depending on the exact electrical properties of each pixel, the uncorrected raw signal will

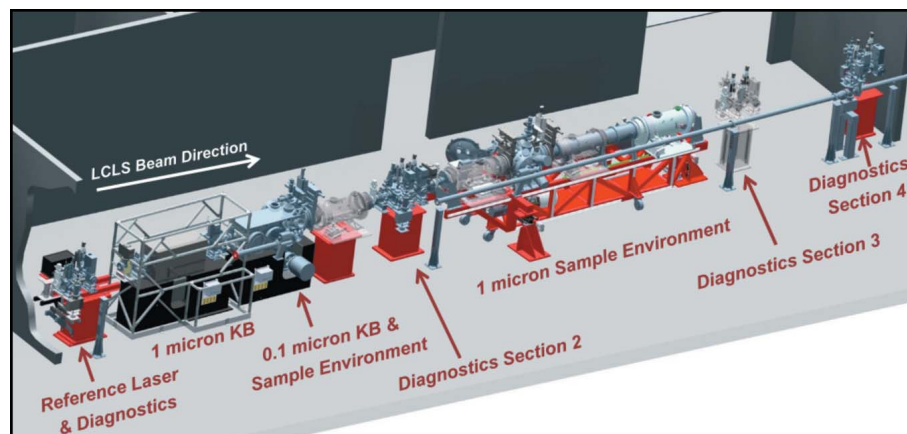


Figure 1
An insight on the beamline setup at CXI. Our experiments took place in the 0.1 μm KB chamber. [Courtesy of SLAC.]

have both a constant offset (the zero value, or pedestal) and a scaling factor (gain) that needs to be calibrated.

In a run with rare or no photon events, the histogram of all the values collected over many events in a single pixel will be centered around an ADU value which represents the zero-photon value. Similarly, when the run contains several photon events, the peak we see after the zero peak is centered on the one-photon value (the gain for that photon energy, see Fig. 3). In a multi-photon regime, additional peaks appear. These are usually roughly proportional to the gain (respectively by a factor of two and three). However, an artifact has previously been described where the discharge of pixels perturbs the reference voltage slightly (Blaj *et al.*, 2015; Herrmann *et al.*, 2013; van Driel *et al.*, 2015). This artifact changes dynamically when photon fluxes change significantly, but can be considered static, included in the gain factor, in the low-flux single particle imaging regime.

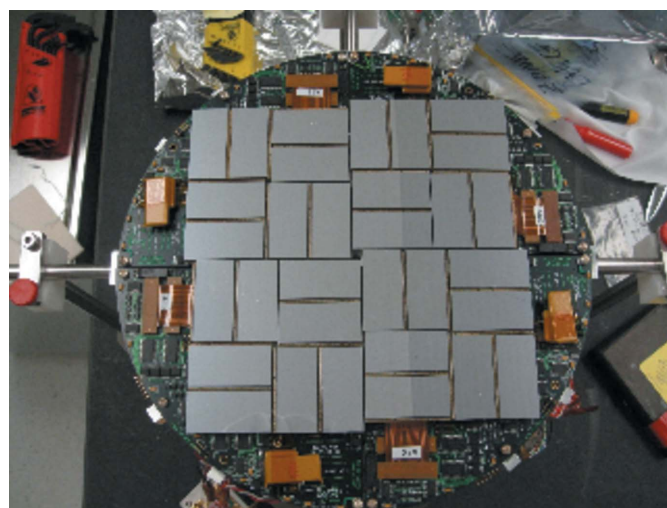


Figure 2
The CSPAD-2.3M consists of 32×1 CSPAD modules, each one further constituted by two ASICs, an ASIC being 185×194 pixels (each of $\sim 110 \mu\text{m} \times 110 \mu\text{m}$). [Courtesy of SLAC/LCLS Detector Group.]

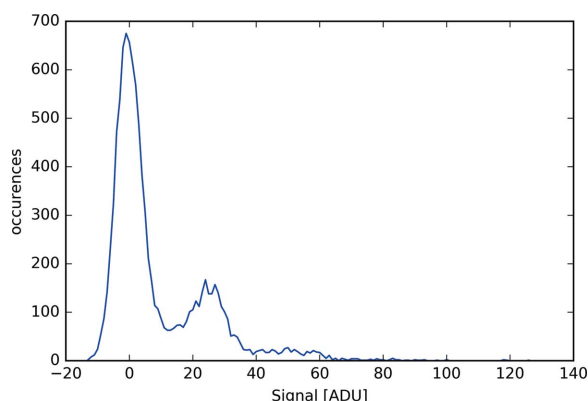


Figure 3
ADU histogram for a single pixel of the back detector in L730 beam time data (run 399), recorded with ongoing injection of sample. The zero photon peak is clearly dominating.

Determining the gain and pedestal correctly is thus crucial to have a reliable photon-counted diffraction pattern.

2. Data processing and analysis

The raw data signals are stored in the proprietary XTC file format, which can be read and manipulated using *PSANA*, a specific environment developed at the LCLS to handle data analysis and extraction. *PSANA* offers a number of calibration and correction steps of direct relevance to photon-counting:

- (i) pedestals;
- (ii) common mode correction per ASIC;
- (iii) gain determination.

2.1. Pedestals

During experiments, so-called dark runs are collected routinely. A dark run captures the detector read-outs without the X-ray source being active. In this way we have an estimate for the electronic noise and other possible X-ray sources not related to the beam (e.g. cosmic rays), by taking the mode of all data in such a run, per pixel. Thus, the most frequent ADU value within this set corresponds to the zero-photon peak (no photons) in a specific pixel.

When collecting full beamline background runs or actual sample diffraction patterns, this typical dark frame can readily be subtracted from those. The dark subtraction term is common for all frames collected after the most recent dark run. Following this pedestal correction, one can choose to apply an additional common mode correction per frame per ASIC.

2.2. Common mode correction per ASIC

Common mode subtraction is needed in order to cancel out frame-wise offsets

in the detector setup. Moreover, as the detector consists of an assembly of different ASICs, this step is performed individually per ASIC, instead of on the overall frame. There is support for several common mode correction modes in *PSANA*, and the current recommended approach can be found here (SLAC Confluence Website, <https://confluence.slac.stanford.edu/display/PSDM/Common+mode+correction+algorithms#Commonmodecorrectionalgorithms-#1-commonmodepeakfindingalgorithm>).

In our processing, we have chosen to define the common mode as nothing but the median of all the values registered in the ASIC for a certain frame. The median was chosen instead of the mode itself (or the arithmetic mean), as it is more statistically robust, especially in the face of correlated single-bit errors, which we have sometimes detected in the CSPAD data we have analyzed. However, in the presence of a strong photon signal over large areas of the detector, the median would no longer accurately represent the zero-photon peak.

After this step, the signal for each pixel is normalized in such a way that the distribution of corrected ADU values is centered around 0 for zero photon events.

2.3. Gain determination

At this point, conventional *PSANA* would identify the zero- and one-photon peak values, fitting them with two distinct Gaussian functions. The quality of the signal, in terms of the ability to discriminate between 0 and 1 photons, can be judged based on the sharpness of the zero-photon peak and the distance, in terms of standard deviations, between this and the one-photon peak.

2.4. Additional detector artifacts and a suggested correction

Despite these corrections for electronic noise and general offset, global frame-wise artifacts can still be present. Some examples are visible in L730 data in Fig. 4 (plot to the left, blue histogram): when looking at dark datasets in the photon count

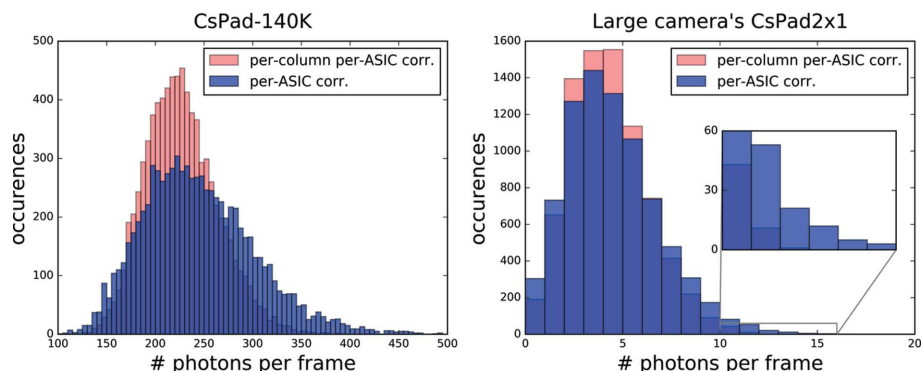


Figure 4
Detector noise histograms for data collected during L730 beam time on the CSPAD-140K detector (left) and for data collected during L867 beam time on one CSPAD 2×1 module in the CSPAD-2.3M (right). For both plots, the x-axis shows the number of photons in each dark frame (representing the detector noise); on the y-axis the number of occurrences of each value in that dataset is found. The correction for a per-ASIC offset is displayed in blue; that for per-column per-ASIC offset is depicted in red. The inset in the right-hand figure shows a larger tail for the per-ASIC offset correction.

space, one can notice a quite broad distribution in photon count ($\mu \simeq 244.10$ and $\sigma \simeq 57.60$).

The structure of the artifact in Fig. 5 (first row), obtained averaging over the sum of 2932 outliers (*i.e.* putative sample hits, if no artifact was expected, percentile 90–95 in photon count to avoid true hits) in the distribution of specific sample runs from L730, suggests a ‘per column’ offset, based on a clearly visible horizontal gradient. More strikingly, this artifact is also observable in the dark data (third row), meaning a systematic bias is present in the CSPAD. Introducing an additional per column, per ASIC common mode correction leads to the result in Fig. 4 (plot to the right, red histogram). The photon count distribution after correcting for the artifact in the dark frames is more well defined with a much-reduced right tail, as would be expected for a run with few or no actual photon events.

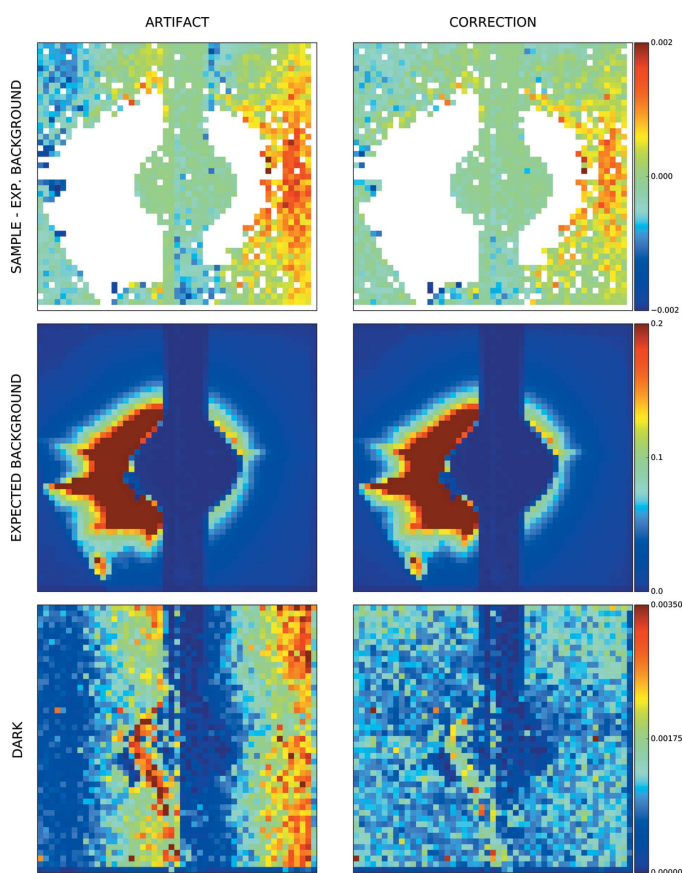


Figure 5

The six patterns represent a downsampled (8×8) average over 2932 frames (first and second row) and over 605 frames (third row). Each row contains frames corrected on a per-ASIC basis (first column) and per-column per-ASIC basis (second column). The first row is representative of the sample runs, where a normalized expected background is subtracted from each frame used for the average; pixels with too high photon counts have been masked out. The second row is the average of the normalized expected background, whereas the last row corresponds to dark run frames. A strong artifact is clearly shown both in the dark data and in the sample runs (band in the right CSPAD 2×1 module in the left images) along with its correction (the respective on the right). The latter is quite striking in the case of dark frames. Data used here come from L730 beam time, specifically runs 399, 410, 423 (sample and expected background) and 398 (dark).

In Fig. 6, the ratio between the standard deviation for the corrected ADU values from a method taking into account a per-ASIC offset and our proposed approach with an additional per-column common mode subtraction is reported, where we take the median value of each ASIC’s column (pixels from top to bottom in Fig. 6) and subtract it from the values in the given column. Since this ratio is above 1 for the vast majority of pixels ($>99.4\%$ for both the detectors), the overall noise level clearly decreases by employing the per-column per-ASIC common mode correction, compared with the simpler per-ASIC baseline. Using the per-ASIC correction, the average per-pixel ADU standard deviations are 2.6252 and 3.9291, whereas with the per-column correction we obtained 2.5942 and 3.8536. Thus, the new correction applied gives an average improvement in the width of the zero-photon peak of $\sim 1.2\%$ for the L867 data and $\sim 1.9\%$ for the L730 dataset.

Despite an improvement of only 1.9% and 1.2% (L730 and L867) in the width of the zero-photon peak, we found a larger difference in false-positive photon reduction: we obtained for L730 a dark run mean photon count $\mu = 244.10$ for the per-ASIC offset correction and $\mu = 226.42$ for the per-column per-ASIC offset correction, but the decrease in spread is far more drastic ($\sigma = 57.60$ and $\sigma = 37.33$, Fig. 4 on the right); for L867, we obtained $\mu \simeq 3.99$ when applying the per-ASIC offset correction, but it decreases to 3.81 when a per-column per-

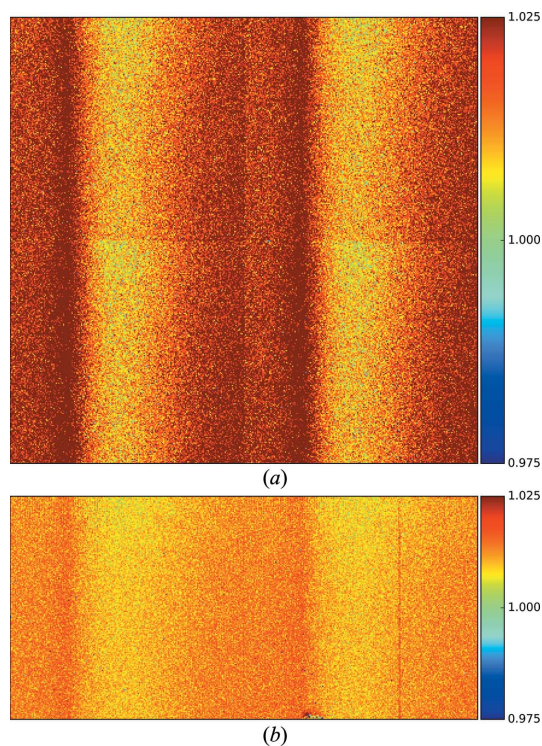


Figure 6

Comparison between per-ASIC and per-column per-ASIC offset correction. The value reported is the ratio between the standard deviation of corrected ADU values for the same dark run using the two methods. The vast majority of values are above 1, meaning that the per-ASIC correction generates more noisy data than per-column per-ASIC approach. (a) Comparison for CSPAD-140K (L730). (b) The same for a single CSPAD 2×1 module in the CSPAD-2.3M (L867).

ASIC offset correction is applied. Even with these low values, the decrease in standard deviation is clear ($\sigma = 2.35$ against $\sigma = 1.99$, Fig. 4 on the left). These effects are not due to reducing overall photon detection power. The average offset imposed over all pixels over all frames was less than 0.0001, implying that the average threshold for photon detection went unchanged and was thus no more restrictive in the per-column offset correction mode.

The reductions in false-positive photon counts can also be represented as a decrease in the false-positive photon detection rate: respectively from 1.70×10^{-3} to 1.58×10^{-3} photon counts $\text{pixel}^{-1} \text{frame}^{-1}$ (standard deviations being 4.00×10^{-4} and 2.60×10^{-4}) and from 5.57×10^{-5} to 5.32×10^{-5} photon counts $\text{pixel}^{-1} \text{frame}^{-1}$ (standard deviations being 3.28×10^{-5} and 2.78×10^{-5}). Therefore, the relative improvements are 7.06% and 4.49% as for the mean rate values; 35.00% and 15.24% as for the standard deviations.

3. Discussion

We have shown a spatially non-uniform sub-structure in the per-frame offset artifact in the CSPAD detectors. We have corrected for this artifact by introducing a separate correction term per-column in the pixel geometry. Based on the patterns visible in Fig. 5 as well as Fig. 6, it seems that this artifact has a specific spatial structure, which is more well ordered than a random offset per column. A further development would be to use the expected profile of the artifact to fit the correction term with greater accuracy. Making such a fit can be of extra importance when photon counts increase, which would make the direct determination of the offset per column challenging. It might be possible to use exclusively the unbound pixels for determining even this spatially non-uniform artifact, if the expected profile for it can be proven to be highly predictable.

4. Conclusions

The flash X-ray imaging technique has been proven to be successful in imaging objects over 40 nm in diameter, with varying degrees of resolution (Daurer *et al.*, 2017; Ekeberg *et al.*, 2015; Hantke *et al.*, 2014; Munke *et al.*, 2016). However, in the context of weak scatterers (biological sample <40 nm in size) collected at CXI, beamline scattering and other sources of background signal have been part of the problem in identifying and analyzing proper particle hits.

We have demonstrated a small, but clear, reduction in the standard deviation of the ADU noise per pixel, using our approach. More importantly, we can see that the resulting effects in falsely detected photons are much more striking. Since hit rates are low in current experiments, and signal is sometimes weak, one of the most important aspects in data processing is to properly separate the background variation from the weakest true sample hits. In this regard, the relative reduction of the standard deviation in false-positive photon counts by up to 35% is our most striking finding. The spread in the background photon count, including falsely detected photons, is an important determinant of suitable thresholds for

performing hit-finding (classifying shots containing sample diffraction *versus* only background) on collected data (Daurer *et al.*, 2017; Hantke *et al.*, 2014).

We believe that all attempts to describe the background and make it consistent will aid further analysis [including attempts to perform three-dimensional reconstruction using *EMC* (Loh & Elser, 2009) on a subset of frames], even in cases when the background cannot be completely eliminated. In the present work we proposed a possible correction by means of which we could decrease the noise level, allowing a superior trade-off between false-positive and false-negatives for the one-photon peak.

Our correction has been explicitly validated on the detectors in use at the CXI instrument, but a similar approach can be transferred to every CSPAD device (including use at the MEC and XCS, in addition to CXI). The improvements suggested are most critical in a strictly photon-counting regime, as in the single-particle imaging case. However, they can also be relevant for serial nanocrystallography, especially if *ab initio* phasing from the diffuse scattering is considered (Ayyer *et al.*, 2016), and for high-resolution imaging, when working with the large CSPAD camera, where the signal on the edges is always fainter (Munke *et al.*, 2016).

Acknowledgements

Data were collected at the Linac Coherent Light Source at the SLAC National Accelerator Laboratory. We thank Andrew Aquila for providing additional details on the L867 experiment and the full SPI collaboration for collecting the data and making it available in the publication of Munke *et al.* Mikhail Dubrovin, Christopher O'Grady, Philip Hart and Gabriella Carini provided significant assistance in clarifying algorithm and instrument issues regarding the CSPAD technology itself, and the algorithm implementation in *PSANA*. We also thank Greg Stewart who designed the CXI end-station picture re-used in Fig. 1. Finally, we would also like to thank Filipe Maia, Janos Hajdu and all other collaborators on the L730 experiment for letting us use the data, and for general support and feedback in the work on the manuscript.

Funding information

The following funding is acknowledged: Vetenskapsrådet (award No. 349-2011-6488).

References

- Ayyer, K., Yefanov, O. M., Oberthür, D., Roy-Chowdhury, S., Galli, L., Mariani, V., Basu, S., Coe, J., Conrad, C. E., Fromme, R., Schaffer, A., Dörner, K., James, D., Kupitz, C., Metz, M., Nelson, G., Xavier, P. L., Beyerlein, K. R., Schmidt, M., Sarrou, I., Spence, J. C. H., Weierstall, U., White, T. A., Yang, J., Zhao, Y., Liang, M., Aquila, A., Hunter, M. S., Robinson, J. S., Koglin, J. E., Boutet, S., Fromme, P., Barty, A. & Chapman, H. N. (2016). *Nature (London)*, **530**, 202–206.
- Barlag, B., Beutel, O., Janning, D., Czarniak, F., Richter, C. P., Kommnick, C., Göser, V., Kurre, R., Fabiani, F., Erhardt, M., Piehler, J. & Hensel, M. (2016). *Sci. Rep.* **6**, 31601.
- Blaj, G., Caragiulo, P., Carini, G., Carron, S., Dragone, A., Freytag, D., Haller, G., Hart, P., Hasi, J., Herbst, R., Herrmann, S., Kenney, C.,

- Markovic, B., Nishimura, K., Osier, S., Pines, J., Reese, B., Segal, J., Tomada, A. & Weaver, M. (2015). *J. Synchrotron Rad.* **22**, 577–583.
- Chapman, H. N., Bajt, S., Barty, A., Benner, W. H., Bogan, M. J., Boutet, S., Cavalleri, A., Duesterer, S., Frank, M., Hajdu, J., Hau-Riege, S. P., Iwan, B., Marchesini, S., Sakdinawat, A., Sokolowski-Tinten, K., Seibert, M. M., Timneanu, N., Truesch, R. & Woods, B. W. (2009). *J. Phys. Conf. Ser.* **186**, 012051.
- Chapman, H. N., Barty, A., Bogan, M. J., Boutet, S., Frank, M., Hau-Riege, S. P., Marchesini, S., Woods, B. W., Bajt, S., Benner, W. H., London, R. A., Plönjes, E., Kuhlmann, M., Treusch, R., Düsterer, S., Tschentscher, T., Schneider, J. R., Spiller, E., Möller, T., Bostedt, C., Hoener, M., Shapiro, D. A., Hodgson, K. O., van der Spoel, D., Burmeister, F., Bergh, M., Caleman, C., Huldt, G., Seibert, M. M., Maia, F. R. N. C., Lee, R. W., Szöke, A., Timneanu, N. & Hajdu, J. (2006). *Nat. Phys.* **2**, 839–843.
- Daurer, B. J., Okamoto, K., Bielecki, J., Maia, F. R. N. C., Mühlhig, K., Seibert, M. M., Hantke, M. F., Nettelblad, C., Benner, W. H., Svenda, M., Timneanu, N., Ekeberg, T., Loh, N. D., Pietrini, A., Zani, A., Rath, A. D., Westphal, D., Kirian, R. A., Awel, S., Wiedorn, M. O., van der Schot, G., Carlsson, G. H., Hasse, D., Sellberg, J. A., Barty, A., Andreasson, J., Boutet, S., Williams, G., Koglin, J., Andersson, I., Hajdu, J. & Larsson, D. S. D. (2017). *IUCrJ*, **4**, 251–262.
- Driel, T. B. van, Herrmann, S., Carini, G., Nielsen, M. M. & Lemke, H. T. (2015). *J. Synchrotron Rad.* **22**, 584–591.
- Ekeberg, T., Svenda, M., Abergel, C., Maia, F. R. N. C., Seltzer, V., Claverie, M., Hantke, M., Jönsson, O., Nettelblad, C., van der Schot, G., Liang, M., DePonte, D. P., Barty, A., Seibert, M., Iwan, B., Andersson, I., Loh, N. D., Martin, A. V., Chapman, H., Bostedt, C., Bozek, J. D., Ferguson, K. R., Krzywinski, J., Epp, S. W., Rolles, D., Rudenko, A., Hartmann, R., Kimmel, N. & Hajdu, J. (2015). *Phys. Rev. Lett.* **114**, 098102.
- Emma, P., Akre, R., Arthur, J., Bionta, R., Bostedt, C., Bozek, J., Brachmann, A., Bucksbaum, P., Coffee, R., Decker, F.-J., Ding, Y., Dowell, D., Edstrom, S., Fisher, A., Frisch, J., Gilevich, S., Hastings, J., Hays, G., Hering, Ph., Huang, Z., Iverson, R., Loos, H., Messerschmidt, M., Miahnahri, A., Moeller, S., Nuhn, H.-D., Pile, G., Ratner, D., Rzepiela, J., Schultz, D., Smith, T., Stefan, P., Tompkins, H., Turner, J., Welch, J., White, W., Wu, J., Yocky, G. & Galayda, J. (2010). *Nat. Photon.* **4**, 641–647.
- Gallagher-Jones, M. & Songa, C. (2014). *SACLA Research Frontiers 2014*. SACLA, SPring-8, Hyogo, Japan.
- Hantke, M. F., Hasse, D., Maia, F. R. N. C., Ekeberg, T., John, K., Svenda, M., Loh, N. D., Martin, A. V., Timneanu, N., Larsson, D. S. D., van der Schot, G., Carlsson, G. H., Ingelman, M., Andreasson, J., Westphal, D., Liang, M., Stellato, F., DePonte, D. P., Hartmann, R., Kimmel, N., Kirian, R. A., Seibert, M. M., Mühlhig, M. M., Schorb, S., Ferguson, K., Bostedt, C., Carron, S., Bozek, J. D., Rolles, D., Rudenko, A., Epp, S., Chapman, H. N., Barty, A., Hajdu, J. & Andersson, I. (2014). *Nat. Photon.* **8**, 943–949.
- Herrmann, S., Boutet, S., Carini, G., Dragone, A., Freytag, D., Haller, G., Hart, P., Herbst, R., Kenney, C., Pines, J. & Williams, G. (2012). *Proceedings of the 12th Pisa Meeting on Advanced Detectors*, La Biodola, Isola d'Elba, Italy, 20–26 May 2012.
- Herrmann, S., Boutet, S., Duda, B., Fritz, D., Haller, G., Hart, P., Herbst, R., Kenney, C., Lemke, H., Messerschmidt, M., Pines, J., Robert, A., Sikorski, M. & Williams, G. (2013). *Nucl. Instrum. Methods Phys. Res. A*, **718**, 550–553.
- Herrmann, S., Hart, P., Dragone, A., Freytag, D., Herbst, R., Pines, J., Weaver, J., Carini, G. A., Thayer, J. B., Shawn, O., Kenney, C. J. & Haller, G. (2014). *J. Phys. Conf. Ser.* **493**, 012013.
- Jamison, S. (2010). *Nat. Photon.* **4**, 589–591.
- Kimura, T., Joti, Y., Shibuya, A., Song, C., Kim, S., Tono, K., Yabashi, M., Tamakoshi, M., Moriya, T., Oshima, T., Ishikawa, T., Bessho, Y. & Nishino, Y. (2014). *Nat. Commun.* **5**, 3052.
- Liang, M., Williams, G. J., Messerschmidt, M., Seibert, M. M., Montanez, P. A., Hayes, M., Milathianaki, D., Aquila, A., Hunter, M. S., Koglin, J. E., Schafer, D. W., Guillet, S., Busse, A., Bergan, R., Olson, W., Fox, K., Stewart, N., Curtis, R., Miahnahri, A. A. & Boutet, S. (2015). *J. Synchrotron Rad.* **22**, 514–519.
- Loh, N. D. & Elser, V. (2009). *Phys. Rev. E*, **80**, 026705.
- Munke, A., Andreasson, J., Aquila, A., Awel, S., Ayyer, K., Barty, A., Bean, R. J., Berntsen, P., Bielecki, J., Boutet, S., Bucher, M., Chapman, H. N., Daurer, B. J., DeMirci, H., Elser, V., Fromme, P., Hajdu, J., Hantke, M. F., Higashiura, A., Hogue, B. G., Hosseinizadeh, A., Kim, Y., Kirian, R. A., Reddy, H. K. N., Lan, T. Y., Larsson, D. S. D., Liu, H., Loh, N. D., Maia, F. R. N. C., Mancuso, A. P., Mühlhig, K., Nakagawa, A., Nam, D., Nelson, G., Nettelblad, C., Okamoto, K., Ourmazd, A., Rose, M., van der Schot, G., Schwander, P., Seibert, M. M., Sellberg, J. A., Sierra, R. G., Song, C., Svenda, M., Timneanu, N., Vartanyants, I. A., Westphal, D., Wiedorn, M. O., Williams, G. J., Xavier, P. L., Yoon, C. H. & Zook, J. (2016). *Sci. Data*, **3**, 160064.
- Neutze, R., Wouts, R., van der Spoel, D., Weckert, E. & Hajdu, J. (2000). *Nature (London)*, **406**, 752–757.
- Robinson, I., Schwenke, J., Yusuf, M., Estandarte, A., Zhang, F., Chen, B., Clark, J., Song, C., Nam, D., Joti, Y., Tono, K., Yabashi, M., Ratnasari, G., Kaneyoshi, K., Takata, H. & Fukui, K. (2015). *J. Phys. B*, **48**, 244007.
- Schot, G. van der, Svenda, M., Maia, F. R. N. C., Hantke, M., DePonte, D. P., Seibert, M. M., Aquila, A., Schulz, J., Kirian, R., Liang, M., Stellato, F., Iwan, B., Andreasson, J., Timneanu, N., Westphal, D., Almeida, F. N., Odic, D., Hasse, D., Carlsson, G. H., Larsson, D. S. D., Barty, A., Martin, A. V., Schorb, S., Bostedt, C., Bozek, J. D., Rolles, D., Rudenko, A., Epp, S., Foucar, L., Rudek, B., Hartmann, R., Kimmel, N., Holl, P., Englert, L., Loh, N. D., Chapman, H. N., Andersson, I., Hajdu, J. & Ekeberg, T. (2015). *Nat. Commun.* **6**, 5704.
- Seibert, M. M., Ekeberg, T., Maia, F. R., Svenda, M., Andreasson, J., Jönsson, O., Odić, D., Iwan, B., Rocker, A., Westphal, D., Hantke, M., DePonte, D. P., Barty, A., Schulz, J., Gumprecht, L., Coppola, N., Aquila, A., Liang, M., White, T. A., Martin, A., Caleman, C., Stern, S., Abergel, C., Seltzer, V., Claverie, J. M., Bostedt, C., Bozek, J. D., Boutet, S., Miahnahri, A. A., Messerschmidt, M., Krzywinski, J., Williams, G., Hodgson, K. O., Bogan, M. J., Hampton, C. Y., Sierra, R. G., Starodub, D., Andersson, I., Bajt, S., Barthelmeß, M., Spence, J. C., Fromme, P., Weierstall, U., Kirian, R., Hunter, M., Doak, R. B., Marchesini, S., Hau-Riege, S. P., Frank, M., Shoeman, R. L., Lomb, L., Epp, S. W., Hartmann, R., Rolles, D., Rudenko, A., Schmidt, C., Foucar, L., Kimmel, N., Holl, P., Rudek, B., Erk, B., Hömke, A., Reich, C., Pietschner, D., Weidenspointner, G., Strüder, L., Hauser, G., Gorke, H., Ullrich, J., Schlichting, I., Herrmann, S., Schaller, G., Schopper, F., Soltau, H., Kühnel, K. U., Andritschke, R., Schröter, C. D., Krasniqi, F., Bott, M., Schorb, S., Rupp, D., Adolph, M., Gorkhover, T., Hirsemann, H., Potdevin, G., Graafsma, H., Nilsson, B., Chapman, H. N. & Hajdu, J. (2011). *Nature (London)*, **470**, 78–81.